Global synchronization and selective desynchronization of FitzHugh-Nagumo oscillators

Labbi, Abderrahim; Milanese, Ruggero; Bosch, Holger

UNIVERSITE DE GENEVE

CENTRE UNIVERSITAIRE
D'INFORMATIQUE
GROUPE VISION

Date: July 15, 1997
N° 97.05

TECHNICAL REPORT

VISION

Global Synchronization and Selective Desynchronization of FitzHugh–Nagumo Oscillators

Abderrahim Labbi Ruggero Milanese Holger Bosch

Computer Vision Group
Computing Science Center, University of Geneva
24 rue du Général Dufour, CH - 1211 Geneva 4 SWITZERLAND
e-mail: labbi@cui.unige.ch

Abstract

In this paper we adopt a correlation approach to neuronal modeling of visual perception, using oscillations. We propose a hierarchy of processing modules corresponding to different levels of representation. The first layer consists of an array of FitzHugh-Nagumo oscillators, which receive a grey–level image as external input. The dynamic behaviour of the coupled oscillators is rigorously investigated and a stimulus-driven synchronization theorem is derived. However, this module reveals itself insufficient to encode correctly and segregate different objects when they have similar grey levels in the input image. Therefore an *attention* mechanism, composed of two further layers is added. The first layer computes a saliency map which extracts a number of salient regions whose average activity greatly differs from their surround. The second layer of the attention mechanism consists of a perturbation map, which computes a positional information on the salient regions and feeds it back to the corresponding groups of oscillators as a one-time *perturbation*. The perturbation signal drives different groups of oscillators to different isochrones, and therefore induces non-zero phase lags between them. Simulation results are presented using real grey–level images.

1 Introduction

A considerable number of neurophysiological findings suggest the hypothesis that brain cells encode information not only by their average firing rate, but also through the precise timing of their firing pattern (Gray et al., 1989; Singer, 1993; Roelfsema et al., 1997). This hypothesis has been supported on computational ground, as one possible way to overcome combinatorial coding strategies, when multiple objects are defined over a multi–dimensional feature space (binding problem) (von der Malsburg and Schneider, 1986; Hopfield, 1995). The basic idea underlying most computational models is that of temporal correlation: two cells encoding the same object establish a relationship by synchronizing their activities, while two cells encoding different objects evolve asynchronously.

In practice, most models employ continuous units exhibiting periodic activity, such as the Wilson–Cowan oscillator, for which a number of analytical results have also been obtained (Wilson and Cowan, 1972; Campbell and Wang, 1996). However, models employing the Wilson–Cowan oscillators appear to have several limitations, both in terms of robustness to input noise and in the presence of graded inputs as shown in the next section.

In this paper we propose a multi–layer architecture (cf. figure 6) based on an alternative neuronal model, the FitzHugh–Nagumo oscillator (FitzHugh, 1961; Nagumo et al., 1962).

Figure 6 about here

The input layer encodes the stimulus, which is a grey–level image. The second layer is a feature map which consists of an array of FitzHugh–Nagumo oscillators. In section 2 we show that, for this model, nice relationships can be established between the value of the external input and the frequency, phase and amplitude of the oscillations. The input from the lower layer is meant to be filtered by some receptive fields, encoding a specific feature, such as edge orientation, color, or shape. For the sake of simplicity we shall henceforth consider a trivial feature map of the same size as the input layer, directly encoding the value of the input unit at the corresponding location. Lateral connections in the feature map link every oscillator to its four neighbours in a Laplacian diffusion scheme. In section 3 we show that, under some constraints on the coupling weights, oscillators receiving the same input asymptotically synchronize, independently of their initial conditions.

This property, although useful to group objects receiving uniform input values, appears unsufficient to discriminate two or more disconnected objects when they possess similar features. This is due to the fact that synchronization depends only on the stimulus intensity but not on the spatial relationships, such as connectivity and position, in the image. In order to take these spatial relationships into account, two further layers are introduced. One, which we call the *attention map*, consists of an array of feature detector units which receive an input signal (the amplitude map) from the oscillators. The receptive field of these units is implemented as a filter whose impulse response is the difference of two Gaussians having different widths. Its goal is to detect connected groups of oscillators whose average amplitude strongly differs from the background (Milanese et al., 1995).

The saliency map is then used to generate spatial information to identify each connected region of the image. This information is computed by an additional layer (the *perturbation map*) which has the same size as the oscillators map. Its units compute the average polar coordinates of all units located in the same attended region; units corresponding to the background are masked to produce zero output. This spatial information is then fed back as a one time perturbation to the oscillators, in order to desynchronize those belonging to different regions, while leaving background units unaffected.

2 The FitzHugh-Nagumo Neuron Model

Before describing the structure and interconnections of the feature map, we first analyze the model used for the basic units, i.e. the FitzHugh-Nagumo oscillator. This model was derived directly from the Hodgkin–Huxley neuron model and is described in (FitzHugh, 1961; Nagumo et al. 1962). A neuron's membrane potential is defined by two coupled variables x (excitation variable) and y

(recovery variable) whose dynamics are given by:

$$\left\{ \begin{array}{ll} \epsilon.\frac{dx}{dt} & = -y - g(x) + I \\ \frac{dy}{dt} & = x - by \ , \end{array} \right. \tag{1}$$

where g is a third order nonlinearity, such as $g(x) = x(x-a)(x-1)$ with $0 < a < 1$, and I is an external input current. The parameter $\epsilon << 1$ controls the relative speed of variation between the variables x and y, x generally varying faster than y (in which case the system is called a relaxation oscillator). The parameters a and b control the asymptotic behaviour of the system for a given input I, as well as the characteristics of the oscillations when they exist (period, amplitude and phase). On the other hand, for fixed a and b, the oscillator dynamics varies according to different values of the input I. Figure 2 shows the system's nullclines for different values of the external input. For more details on the bifurcation analysis of the FitzHugh-Nagumo neuron model, the interested reader is referred to (Murray, 1993; Troy, 1976; Rajasekar and Lakshmanan, 1994).

Figure 2 about here

For small values of the input ($I < I_1$), the system relaxes to a stable attractor state (stable equilibrium) since the eigenvalues of the linearized system around the singularity have negative real parts. When $I = I_1$, the eigenvalues have zero real parts; consequently, the fixed point is no longer stable and bifurcates into a small amplitude limit cycle as I is increased. This is a typical supercritical Hopf bifurcation and the period of the limit cycles corresponding to I in the vicinity of I_1 may be approximated by $T = \frac{2\pi}{\omega}$, where ω is the imaginary part of the eigenvalue of the Jacobian at the singularity associated to $I = I_1$. In figure 3 we show how the amplitude and frequency of the oscillation vary as a function of I. It can be seen that, for a large interval of I in the vicinity of the bifurcation, the amplitude is monotonic in I while the frequency is nearly constant. Figure 3 illustrates two typical phenomena which are generally observed for a supercritical Hopf bifurcation: the amplitude of the oscillations grows continuously from zero and proportional to $\sqrt{\mu - \mu_1}$, where μ is the trace of the Jacobian at the singularity, while the frequency of the oscillation may be approximated by $\omega = det(J_1)$, where $det(J_1)$ is the determinant of the Jacobian at the bifurcation (Strogatz, 1994).

Figure 3 about here

The above observations can also be derived analytically using the gradient-Hamiltonian decomposition of a system of differential equations. Given a continuous 2D differential system,

$$\left\{ \begin{array}{ll} \frac{dx}{dt} & = F(x,y) \\ \frac{dy}{dt} & = G(x,y) \end{array} \right. \tag{2}$$

the Francoise-Saito theorem (Francoise, 1980) states that, around a singularity, it can be uniquely decomposed as follows:

$$\left\{ \begin{array}{lllll} \frac{dx}{dt} & = -\frac{\partial}{\partial x}V(x,y) & - \ \frac{\partial}{\partial y}H(x,y) & + \ R_1(x,y) \\ \frac{dy}{dt} & = -\frac{\partial}{\partial y}V(x,y) & + \ \frac{\partial}{\partial x}H(x,y) & + \ R_2(x,y) \ , \end{array} \right. \tag{3}$$

where $V(x,y)$ is a dissipative potential which defines the gradient part of the dynamics, and $H(x,y)$ is a conservative potential representing the Hamiltonian part. $R_i(x,y)$ is a residue which tends to zero as (x,y) tends to the singularity.

A conjecture by Thom-Sebastiani (Thom, 1978; Demongeot et al., 1988) states that there also exists a mixed gradient-Hamiltonian decomposition of any 2D differential system, when the singularity is replaced by an attractor or repellor, particularly for a limit cycle. In the case of FitzHugh-Nagumo system (1), one can easily derive such a decomposition with zero residue using simple integration. If we consider the following potentials,

$$\begin{array}{rcl} V(x,y) & = & \frac{1}{2}by^2 + \frac{1}{4}\mu x^4 - \frac{1}{3}(1+a)\mu x^3 + \frac{1}{2}\mu a x^2 - \frac{I}{2}\mu x \\ H(x,y) & = & \frac{1}{2}\mu y^2 + \frac{1}{2}x^2 - \frac{I}{2}\mu y \ , \end{array} \tag{4}$$

where $\mu = (\epsilon)^{-1}$, then one can easily verify that the system (1) can be written as

$$\begin{cases} \frac{dx}{dt} &= -\frac{\partial}{\partial x}V(x,y) \;-\; \frac{\partial}{\partial y}H(x,y) \\ \frac{dy}{dt} &= -\frac{\partial}{\partial y}V(x,y) \;+\; \frac{\partial}{\partial x}H(x,y) \;. \end{cases} \tag{5}$$

Due to the conservative property of H, the Hamiltonian dynamics at a point (x, y) tends to move the trajectory of the system (5) along the level curve of H defined by $\mathcal{C} = H(x, y)$. Conversely, the dissipative property of the gradient tends to move the trajectory towards the minimum of V, and to bring the trajectory around such minimum under the influence of the Hamiltonian dynamics. A detailed analysis of the frequency and amplitude of oscillations, by way of the Hamiltonian part of the dynamics, will be developed in a subsequent paper.

The above dependency between of the amplitude and frequency on the input signal is particularly important for information encoding. When the input is binary (stimulus present or absent) a correspondence is in general straightforward, since one only needs to have a limit cycle for the stimulus and a fixed point in the absence of a stimulus. To this end, Wilson–Cowan oscillators appear suitable (Campbell and Wang, 1996). However, in our study we are interested in modeling continuous input represented by a grey–level image. In this case, it is essential to establish a one–to–one continuous mapping between the input and the period and/or amplitude of the resulting oscillations. The FitzHugh–Nagumo model satisfies this property, thanks to the monotonic dependency between the input and the oscillation amplitude. Furthermore, the almost constant frequency is also an attractive property, in view of the possibility of synchronizing oscillators coding for the same object but receiving different inputs. As shown in figure 4, this property is missing in the Wilson–Cowan oscillator whose frequency depends nonlinearly on the input (figure 4, dashed curve), therefore making synchronization harder.

Figure 4 about here

3 Synchronization of Coupled FN Oscillators

In this section we present a theoretical result on the stimulus-driven synchronization of coupled FitzHugh-Nagumo oscillators. We prove the following theorem in the case of an open chain of oscillators which are symmetrically–coupled with nearest–neighbor connections between x and y units (cf. figure 5).

Figure 5 about here

Theorem. *Given an open chain of N coupled FitzHugh-Nagumo oscillators $\{(x_i, y_i), i = 1, .., N\}$ receiving the same input $I_i = I, i = 1, .., N$, and whose dynamics are described by:*

$$\begin{cases} \frac{dx_i}{dt} &= -y_i - g(x_i) + I_i + \alpha(x_{i-1} - x_i) + \alpha(x_{i+1} - x_i) \;,\; i = 2, ..., N-1 \\ \frac{dy_i}{dt} &= x_i - by_i + \beta(y_{i-1} - y_i) + \beta(y_{i+1} - y_i) \;, \end{cases} \tag{6}$$

with boundary conditions:

$$\begin{cases} \frac{dx_1}{dt} &= -y_1 - g(x_1) + I_1 + \alpha(x_2 - x_1) \\ \frac{dy_1}{dt} &= x_1 - by_1 + \beta(y_2 - y_1) \\ \frac{dx_N}{dt} &= -y_N - g(x_N) + I_N + \alpha(x_{N-1} - x_N) \\ \frac{dy_N}{dt} &= x_N - by_N + \beta(y_N - y_{N-1}) \;, \end{cases} \tag{7}$$

the oscillators asymptotically synchronize with zero phase shift provided that α and β satisfy the following conditions:

$$\begin{cases} \alpha > \frac{1}{2}(1 + 2\beta\cos(\pi/N)) \\ \beta > \frac{1}{2(1-cos(\pi/N))} \\ \beta \geq \alpha \;. \end{cases} \tag{8}$$

Proof: The basic idea of the proof is to show that, $\forall\ i, r_i^2 = (x_i - x_{i+1})^2 + (y_i - y_{i+1})^2$ tends to zero asymptotically for any initial conditions. Let us first consider the following variable change:

$$x_i - x_{i+1} = r_i \cos(\theta_i)\ ,\ y_i - y_{i+1} = r_i \sin(\theta_i)\ ,\ i = 1, ..., N-1\ ,\ r_i \geq 0\ , \theta_i \in [0, 2\pi[. \tag{9}$$

Then, differentiating $\frac{1}{2} r_i^2 = \frac{1}{2}(x_i - x_{i+1})^2 + (y_i - y_{i+1})^2$ with respect to time gives,

$$\begin{aligned} r_i.\dot{r}_i &= \frac{dr_i^2}{2dt} = \frac{d}{2dt}[(x_i - x_{i+1})^2 + (y_i - y_{i+1})^2] \\ &= (x_i - x_{i+1})(\dot{x}_i - \dot{x}_{i+1}) + (y_i - y_{i+1})(\dot{y}_i - \dot{y}_{i+1}) \\ &= (x_i - x_{i+1})[-(y_i - y_{i+1}) - (g(x_i) - g(x_{i+1})) + \alpha(x_{i-1} - x_i) - 2\alpha(x_i - x_{i+1}) \\ &+ \alpha(x_{i+1} - x_{i+2})] + (y_i - y_{i+1})[(x_i - x_{i+1}) - b(y_i - y_{i+1}) + \beta(y_{i-1} - y_i) \\ &- 2\beta(y_i - y_{i+1}) + \beta(y_{i+1} - y_{i+2})]\ . \end{aligned} \tag{10}$$

Using simple algebra, it is easy to show that

$$-(x_i - x_{i+1})(g(x_i) - g(x_{i+1})) \ \leq\ (x_i - x_{i+1})^2 \ \leq\ r_i^2. \tag{11}$$

By assuming $\alpha \leq \beta$, the following inequalities hold:

$$\begin{aligned} \alpha \cos(\theta_i)\cos(\theta_{i+1}) + \beta \sin(\theta_i)\sin(\theta_{i+1}) &\leq \beta r_i r_{i+1} \\ \alpha \cos(\theta_i)\cos(\theta_{i-1}) + \beta \sin(\theta_i)\sin(\theta_{i-1}) &\leq \beta r_i r_{i-1}\ . \end{aligned} \tag{12}$$

Therefore, after some developments and simplifications, the previous system can be rewritten in (r_i, θ_i) coordinates as:

$$\begin{aligned} r_i.\dot{r}_i &= -r_i \cos(\theta_i)(g(x_i) - g(x_{i+1})) - b r_i^2 \sin(\theta_i)^2 - 2\alpha r_i^2 \cos(\theta_i)^2 - 2\beta r_i^2 \sin(\theta_i)^2 \\ &+ r_i r_{i-1}(\alpha \cos(\theta_i)\cos(\theta_{i-1}) + \beta \sin(\theta_i)\sin(\theta_{i-1})) + r_i r_{i+1}(\alpha \cos(\theta_i)\cos(\theta_{i+1}) \\ &+ \beta \sin(\theta_i)\sin(\theta_{i+1})) \\ &\leq r_i^2 - 2\alpha r_i^2 + \beta r_i r_{i-1} + \beta r_i r_{i+1}\ . \end{aligned} \tag{13}$$

Now let us consider the linear differential system defined by

$$\dot{q}_i = (1 - 2\alpha) q_i + \beta q_{i-1} + \beta q_{i+1}\ \ ,\ i = 1, ..., N-1\ , \tag{14}$$

which can be rewritten as $\dot{\mathbf{q}} = A\mathbf{q}$ where $\mathbf{q} = (q_1, q_2, ..., q_{N-1})$, and the $N \times N$ matrix A is:

$$A = \begin{pmatrix} (1-2\alpha) & \beta & & & \\ \beta & (1-2\alpha) & \beta & & \\ & \ddots & \ddots & \ddots & \\ & & \beta & (1-2\alpha) & \beta \\ & & & \beta & (1-2\alpha) \end{pmatrix}\ . \tag{15}$$

From the inequality (13), we have $\dot{\mathbf{r}} \leq \dot{\mathbf{q}}$ for any initial condition $\mathbf{r}(0) = \mathbf{q}(0)$.Therefore $\mathbf{r}(t)$ is bounded by $\mathbf{q}(t)$. Since $\mathbf{r}(t) \geq 0$, to show that $\mathbf{r}(t)$ tends to zero asymptotically, it suffices to show that this is true for $\mathbf{q}(t)$. The problem hence amounts to finding conditions under which the matrix A is stable, i.e. all its eigenvalues have negative real parts. Since A is a triangular Toeplitz matrix (Barnett, 1990), its eigenvalues are:

$$\lambda_k = 1 - 2\alpha + 2\beta \cos(k\pi/N)\ ,\ k = 1, ..., N-1\ , \tag{16}$$

with $\lambda_{N-1} < \lambda_{N-2} < ... < \lambda_1$. To garantee negative eigenvalues, it suffices to impose $1 - 2\alpha + 2\beta\cos(\pi/N) < 0$, i.e. $1 + 2\beta\cos(\pi/N) < 2\alpha$. Since we assumed $\alpha \leq \beta$, this reduces to $1 + 2\beta\cos(\pi/N) \leq 2\beta$, which implies the condition, $\beta \geq \frac{1}{2(1-\cos(\pi)/N)}$, and ends the proof.

The synchronizing dynamics of the system may be intuitively interpreted as follows. For any given initial conditions on (x_i, y_i), the coupling terms $\alpha(x_{i-1} - 2x_i + x_{i+1})$ and $\beta(y_{i-1} - 2y_i + y_{i+1})$, which are proportional to the difference between two neighboring oscillators, are large enough to

drive the oscillators towards neighboring fixed points. Eventually, the difference between the oscillators will decrease below some bifurcation threshold. Then oscillators with identical inputs will adjust minor differences in their phases, due to the coupling term, to reach zero–lag synchronization.

When the chain is replaced with a 2–D array of oscillators, we have observed experimentally (through extensive simulations) the same stimulus–driven synchronization property.

One can readily see from the constraints of the previous theorem that the values of α and β are monotonically increasing in N. However, simulations revealed that much smaller values are sufficient to achieve synchronization, and that one can safely employ $\alpha \leq \beta < 1$, as has been done for all simulations presented in this paper ($\alpha = \beta = 0.05$). Indeed, the above conditions are sufficient but not necessary, and better upper bounds may possibly be found. Similar observations can be made for a closely related result (Campbell and Wang, 1996) who derived coupling conditions which are sufficient to synchronize a chain of piece-wise linearized Wilson-Cowan oscillators.

4 Desynchronization Through Selective Attention

As shown in section 2, the information carried by a FitzHugh–Nagumo oscillator lies in its phase and amplitude, whereas the frequency remains approximatly constant. During simulations, we observed a global synchronization behavior of the oscillators, i.e. each neuron oscillates with approximatly the same frequency and phase, altough it encodes its own input by the amplitude. This leaves the amplitude as the only information available to separate multiple objects. However, if two disconnected objects have the same intensity in the input image, the two corresponding groups of oscillators will synchronize their activities.

We therefore introduce an *attention* mechanism which carries spatial information and selectively modifies the phases of disconnected groups of oscillators. Such a mechanism is implemented by the two upper layers of the architecture (cf. figure 6). The first one is the saliency map, which selects connected groups of feature map oscillators whose amplitudes exhibit high contrast from their surround. The second layer is the perturbation map, whose goal is to compute a desynchronizing feedback signal for the feature map oscillators located in the extracted salient regions.

4.1 The Saliency Map

This map consists of feature detector units computing the convolution of the oscillators amplitudes with a *difference of two Gaussians*, which corresponds to a very common receptive field type in the striate cortex, as well as in the thalamus and the superior colliculus. The two latter brain areas have been hypothesized to play a central role in selective attention and eye movements (Crick, 1984; Desimone et al., 1990). The goal of the saliency layer is to detect blob–like groups of feature map oscillators whose amplitudes greatly differ from their surround. These groups of oscillators correspond to regions in the image most likely to contain objects of interest to human subjects (Koch and Ullman, 1987; Duncan and Humphreys, 1989).

The activity of a unit s_{ij}, at position (i,j), $i,j = 1,...,N$, is thus defined by thresholding the rectified output of the convolution between the oscillator amplitudes a_{ij} and a difference–of–Gaussians (DoG) filter F. The amplitudes a_{ij} are computed from the x_{ij} variables of the oscillators after a transient $T_a = 2 \cdot T$, where T is the FN oscillators average period:

$$\begin{aligned} u_{ij} &= \sum_{m=1}^{N} \sum_{n=1}^{N} a_{mn} \cdot F_{i-m,j-n} \\ F_{ij} &= \exp -\frac{i^2+j^2}{\sigma^2} - c \cdot \exp -\frac{i^2+j^2}{d\sigma^2} \\ s_{ij} &= H(u_{ij} - \vartheta) + H(-u_{ij} - \vartheta) \end{aligned} \tag{17}$$

where c is a weight guaranteeing equal integrals of the two gaussians over the bounded, discrete image domain, σ is the width of the positive (*on*) Gaussian, d is the *off/on* ratio, and H is the Heaviside function, with offset ϑ. In the simulations presented in this paper, the following values have been used for these parameters, $\sigma = 8, d = 8, N = 128, \vartheta = 30$; the image size is 128×128.

Due to the band-pass filter F, its convolution with the amplitude map (i.e. the values u_{ij}) presents a number of peaks, corresponding to regions of oscillators having similar amplitudes to each other and different amplitudes from the surrounding region. The role of the units s_{ij} is to represent the objects' shape in the feature map by simply thresholding the filter response, thereby segmenting them from the background. It is important to note that these feature detectors are insensitive to the absolute input levels of the background and foreground objects, and depend only on their difference.

This saliency map can more easily be used to generate a selective feedback for the feature map oscillators. Figure 6 shows an example image containing three foreground shapes over a textured background, together with the corresponding amplitude and saliency maps.

Figure 6 about here

4.2 The Perturbation Map

Desynchronization between different oscillator groups, selected by the saliency map, is attained by introducing an additional layer of units called the *perturbation map* (cf. figure 6). Each unit in this layer needs to identify uniquely the group to which it belongs. We do so by encoding positional information about the region occupied by each group. Therefore, each unit $\mathbf{p}_{ij} = (r_{ij}, \theta_{ij})$ is initialized with the polar coordinates of position (i, j), and in order to have all units corresponding to a same group of oscillators pointing to the same region, we employ the following anisotropic diffusion dynamics:

$$\begin{cases} \eta \frac{d\mathbf{p}_{ij}}{dt} & = -\mathbf{p}_{ij} + \frac{1}{\sum_{m,n \in \mathcal{N}(i,j)} a_{mn}} \sum_{m,n \in \mathcal{N}(i,j)} \mathbf{p}_{mn} \cdot a_{mn} \\ \mathbf{p}_{ij}(0) & = (\sqrt{\frac{(i^2+j^2)}{2 \cdot N^2}} \ , \ \arctan(j/i)) \cdot a_{ij} \ , \end{cases} \tag{18}$$

where $\mathcal{N}(i, j)$ is the set of the four nearest neighbours of unit $\mathbf{p}_{ij}$. Due to the initial conditions of $\mathbf{p}_{ij}$, the system converges to the following configuration: the values of units $\mathbf{p}_{ij}$ located in the background are zero since $a_{ij} = 0$; units $\mathbf{p}_{ij}$ belonging to the same connected foreground region R will tend to a same average value of $\{ (r_{ij}, \theta_{ij}) \ , (i,j) \in R \}$; units located in two different foreground regions will converge to different values. Asymptotically, the values of the desynchronizing map thus contain the necessary information to generate a desynchronizing feedback.

By selecting a large relaxation speed η in eq. (18), the convergence of the desynchronizing map is accelerated, since it does not depend on a varying input. The diffusion process can thus be stopped at a finite time such as $T_p = 4 \cdot T$. The temporal evolution of the perturbation map units (θ_{ij} components), for the input image shown in figure 6 (left), is reported in figure (7).

Figure 7 about here

Given the perturbation map, a feedback must be generated for the corresponding units of the feature map oscillators. In order to illustrate the effect of different perturbations on the oscillators phases, it is useful to draw the isochrones of a FN oscillator (figure 8). An isochrone is the set of all initial conditions (x, y) such that all uncoupled oscillators initialized with with any of these values asymptotically synchronize with zero phase lag. Therefore, if one wants to impose a certain phase lag between two oscillators, it suffices that they be perturbated in such a way that they restart their dynamics at different isochrones.

Figure 8 about here

In our case, the vectors $\mathbf{p}_{ij}(T_p)$ computed by the perturbation map will be fed back to oscillators in the corresponding regions of the feature map as a one–time additive perturbation at time T_p. The x_{ij}, $i, j = 1, ..., N$, components of the oscillators are additively perturbated by the r_{ij} values, while the y_{ij} variables are perturbated by the θ_{ij} values:

$$\begin{cases} x_{ij}(T_p) & = & x_{ij}(T_p) + \delta_1 \cdot r_{ij}(T_p) \\ y_{ij}(T_p) & = & y_{ij}(T_p) + \delta_2 \cdot \theta_{ij}(T_p), \end{cases} \tag{19}$$

where δ_1 and δ_2 are weighting coeffcients. Since for disconnected regions the perturbation values are different, the effect of the feedback is to drive oscillators belonging to different regions in the phase space corresponding to different isochrones. Due to the relaxation property of the FN oscillator, the isochrones are nearly horizontal while far away from the cycle. This means that, to desynchronize two oscillators, only a perturbation of the y variable is useful whereas perturbating only along the x direction would still leave the oscillators on the same isochrone. However, in the proximity of the limit cycle, the shape of the isochrones is more complex, and perturbations both in the x and y directions are more convenient for desynchronization. To this end, the value of α in eq. (19) should not be large. In our simulations, we used $\delta_1 = \delta_2 = 3$.

After the perturbation, the system will continue to evolve according to coupled oscillators' dynamics but with a certain phase lag between different groups of oscillators.

Figure 9 shows the activity diagram of the x variables of the oscillators, before and after perturbation at time $T_p = 6$, for the input image presented in figure 6 (left).

Figure 9 about here

5 Experimental Results

In this section we present the results obtained on two additional real images, containing multiple objects on a noisy background.

Figure 10 about here

The input images (figure 10.a) are 128×128 grey–level images containing multiple objects. Every oscillator at location (i, j), $i, j = 1, .., 128$, in the feature map receives, as external input, the corresponding pixel intensity I_{ij}. After a transient $T_a = 2 \cdot T$, the oscillators stabilize their behaviour, and the saliency map is computed (figure 10.b). The saliency map is then fed into the perturbation map whose units compute the perturbation values associated to the salient regions during a time interval of two oscillator's periods. At time $T_p = 4 \cdot T$, the perturbation values are fed back to the oscillators as a one time additive perturbation in order to drive different groups of oscillators to different isochrones, therefore causing a phase lag between such groups. To quantify the induced desynchronization, figures 10.c and 10.d show the cross-correlation diagrams between units of different objects before and after the perturbation. These diagrams indicate that different foreground objects can easily be discriminated from each other. However, it is also important to verify that oscillators in a foreground object can also be discriminated from the background. In figure 11, we show the cross–correlation diagrams between oscillators located in foreground objects and in the background of figure 6 (left). In order to draw a valid conclusion, we considered the worst case scenario which consists of picking for an oscillator in the foreground, one oscillator in the background which receives the same external input.

Figure 11 about here

In order to quantify the desynchronizing role of the perturbations we analyzed the cross–correlation among x variables of the oscillators (figures 10(d) and 11). For any two units x_u, x_v we define the normalized cross–correlation index over an interval $[T_1, T_2]$ as:

$$\rho_{T_1}^{T_2}(u, v) = \frac{\mathrm{E}_{T_1}^{T_2}[x_u x_v] - \mathrm{E}_{T_1}^{T_2}[x_u]\mathrm{E}_{T_1}^{T_2}[x_u]}{\sqrt{\mathrm{E}_{T_1}^{T_2}[x_u^2] - \mathrm{E}_{T_1}^{T_2}[x_u]^2} \cdot \sqrt{\mathrm{E}_{T_1}^{T_2}[x_v^2] - \mathrm{E}_{T_1}^{T_2}[x_v]^2}} \ , \tag{20}$$

where $\mathrm{E}_{T_1}^{T_2}[x] = \int_{T_1}^{T_2} x(t)dt$. Note that this index takes values in the interval $[-1, 1]$, whose extrema indicate perfect desynchronization/synchronization respectively. For the simulation described in figure (10.a (top)), we defined the time interval $[2, 6]$ before perturbation and the interval $[8, 12]$ after perturbation. We selected two x units for each object: x_1^b, x_2^b for the teddy bear, x_1^c, x_2^c for the cup, and x_1^d, x_2^d for the duck (top left corner of the image). First, we computed ρ before perturbation. The average value of ρ within objects is very high, namely 0.98. However, the

cross-correlation between objects is also high (0.94), despite the amplitude differences among different objects. This is due to the normalized cross-correlation, which discounts from each signal's amplitude. We then computed the cross-correlation index in the post–perturbation interval. The desynchronizing role of the perturbation clearly appears by evaluating ρ across different objects, the average cross-correlation index decreasing from 0.94 to 0.44.

These results indicate that the proposed system successfully achieves spatio-temporal object segmentation in real images provided that foreground objects exhibit sufficient contrast from the background. Oscillators representing the same object synchronize their activities, while oscillators representing different objects are desynchronized thanks to the *top–down* attention mechanism. Furthermore, oscillators in a foreground object are desynchronized with oscillators in the background. The foreground objects can then be easily labeled in the oscillators amplidude and phase space.

6 Discussion and Related Work

The present paper adresses a central application of the temporal correlation approach to visual modeling, which concerns image segmentation using continuous oscillators. Several previous studies have adressed the same issue, using networks of Wilson-Cowan oscillators (von der Malsburg and Buhmann, 1992; Wang, 1995; Campbell and Wang, 1995; Vorbruggen and von der Malsburg, 1995), or a time-delayed version of such oscillators (Schillen and Koenig, 1994). However, these architectures are quite complex in the sense that the input stimulus is encoded by employing as many networks of oscillators as there are grey levels in the input image. In fact these oscillators receive only binary inputs, whereas we have shown that FitzHugh-Nagumo units allow the establishment of a one-to-one mapping between a graded input and the oscillation amplitude, and that synchronization is achieved using simple nearest-neighbor connections. Another highly related work is the LEGION system, described in (Terman and Wang, 1995; Wang and Terman, 1997), which consists of a network of locally connected (through the x variable only) relaxation oscillators which form groups of synchronized oscillators competing through a global inhibitor. The interactions (lateral and through the global inhibitor) between oscillators in such networks are mainly due to a *selective gating* process, which is based on the fast threshold modulation introduced in (Somers and Kopell, 1995). The LEGION system exhibits a rapid synchronization dynamics and achieves segmentation of real grey–level images, although it seems to be sensitive to the initial conditions of the oscillators.

Although the FN oscillator properties shown in this paper can be exploited for perceptual grouping in noisy images, they appear insufficient to segment multiple objects containing large input variations. To this end, we introduced an attention mechanism for selecting regions of interest in the image, and then generating a feedback signal to selectively modify the oscillators phases.

Several lines of improvements of the present study are under investigation. The oscillators dynamics when the input stimulus is modeled by the response of Gabor filters is being studied, in order to construct an illumination–invariant shape representation. Also, the isotropic connectivity between oscillators (i.e. nearest–neighbor coupling with fixed weights) should be enhanced in a way which reflects the contrast variation in the input image. This would require a dynamic coupling approach based on discretizations of anisotropic reaction-diffusion operators (Berthommier et al., 1991; Cottet, 1994).

References

[1] Barnett, S.: *Matrices: Methods and Applications.* Clarendon Press: London (1990).

[2] Berthommier, F., et al.: Asymptotic Behavior of Neural Networks and Image Processing. In Babloyantz, A. (Editor), *Self-Organization, Emerging Properties, and Learning.* Plenum Press, New York, 1991, 219–229.

[3] Campbell, S., Wang, D.: Synchronization and Desynchronization in a Network of Locally Coupled Wilson-Cowan Oscillators. *IEEE Trans. on Neural Networks*, **7:3**, 1996, 541–554.

[4] Cottet, G.H.: Neural Networks: Continuous Approach and Applications to Image Processing. Institut national Polytechnique de Grenoble, France, Technical Report LMC-IMAG, RT 113, 1994.

[5] Crick, F.: Function of the Thalamic Reticular Complex: the Searchlight Hypothesis. *Proc. of the National Academy of Sciences*, 1984, **81**, 4586-4590.

[6] Demongeot, J., Estève, F., Pachot, P.: Comportement Asymptotique des Systèmes: Applications en Biologie. *Rev. Int. Syst.*, **2**, 1988, 417.

[7] Desimone, R. et al.: Attentional Control of Visual Perception: Cortical and Subcortical Mechanisms. *Cold Spring Harbor Symp. on Quant. Biol.*, **LV**, 1990, 963-971.

[8] Duncun, J., and Humphreys, G.W.: Visual Search and Stimulus Similarity. *Psychological Review*, **96(3)**, 1989, 433-458.

[9] FitzHugh, R.: Impulses and Physiological States in Models of Nerve Membrane. *Biophys. Journal*, **1**, 1961, 445-466.

[10] Francoise, J.P.: Systèmes Maximaux d'une Singularité Quasi–homogène. *C. R. Acad. Sc.*, **290**, 1980, 1061-1065.

[11] Gray, C.M., et al.: Oscillatory Responses in Cat Visual Cortex Exhibit Inter-Columnar Synchronization which Reflects Global Stimulus Properties. *Nature*, **338**, 1989, 334–337.

[12] Hopfield, J.J.: Pattern Recognition Computation Using Action Potential Timing for Stimulus Representation. *Nature*, **376**, 1995, 33–36.

[13] Labbi, A., et al.: A Network of FitzHugh–Nagumo Oscillators for Object Segmentation. *International Symposium on Nonlinear Theory and Applications (NOLTA'97)*, Nov. 29 – Dec. 3 1997, Hawaii, (to appear).

[14] Koch, C., and Ullman, S.: Shifts in Selective Visual Attention: Towards the Underlying Neural Circuitry. In L.M. Vaina (ed.), *Matters of Intelligence*, Reidel Publishing, 1987, 115-141.

[15] von der Malsburg C., and Schneider, W.: A Neural Cocktail-Party Processor. *Biological Cybernetics*, **54**, 1986, 29–40.

[16] von der Malsburg C., and Buhmann, J.: Sensory Segmentation with Coupled Neural Oscillators. *Biological Cybernetics*, **67**, 1992, 233–242.

[17] Milanese R. et al.: Attentive Mechanisms for Dynamic and Static Scene Analysis. *Optical Engineering*, **34(8)**, 1995, 2428–2434.

[18] Murray, J.D.: *Mathematical Biology*. 2nd edition (1993), Springer.

[19] Nagumo, J.S., Arimoto, S., Yoshizawa, S.: An Active Pulse Transmission Line Simulating Nerve Axon. *Proc. of IRE*, **50**, 1962, 2061–2071.

[20] Rajasekar, S., Lakshmanan, M.: Bifurcation, Chaos and Suppression of Chaos in FitzHugh–Nagumo Nerve Conduction Model equation. *J. Theor. Biology*, **166**, 1994, 275–288.

[21] Roelfsema, P.R., et al.: Visuomotor Integration is Associated with Zero Time-lag Synchronization among Cortical Areas. *Nature*, **385**, January 1997, 157-161.

[22] Schillen, T.B., Konig, P.: Binding by Temporal Structure in Multiple Feature Domains of an Oscillatory Neuronal Network. *Biological Cybernetics*, **70**, 1994, 397–405.

[23] Singer, W.: Synchronization of Cortical Activity and its Putative Role in Information Processing and Learning. *Annual Review of Physiology*, **55**, 1993, 349–374.

[24] Somers, D. and Kopell, N.: Waves and Synchrony in Networks of Oscillators of Relaxation and Non-relaxation Type. *Physica D*, **89**, 1995, 169–183.

[25] Strogatz, H.S.: *Nonlinear dynamics and Chaos.* Addison-Wesly Publ. (1994).

[26] Terman, D. and Wang, D.L.: Global Competition and Local Cooperation in a Network of Neural Oscillators. *Physica D*, **81**, 1995, 148–176.

[27] Thom, R.: Modèles Mathématiques de la Morphogenèse. *Edisciences*, Paris, 1978.

[28] Troy, W.C.: Bifurcation Phenomena in FitzHugh's Nerve Conduction Equations. *Journal of Math. Analysis and Applications*, **54**, 1976, 678–690.

[29] Vorbruggen, J.C., von der Malsburg, C.: Data-Driven Segmentation of Grey-Level Images with Coupled Nonlinear Oscillators. *Proc. of ICANN'95*, Paris, 299–302.

[30] Wang, D.L.: Emergent Synchrony in Locally Coupled Neural Oscillators. *IEEE Trans. on Neural Net.*, **6(4)**, 1995, 941–948.

[31] Wang, D.L. and Terman, D.: Image Segmentation Based on Oscillatory Correlation. *Neural Computation*, **9**, 1997, 805–836.

[32] Wilson, H.R., Cowan, J.D.: Excitatory and Inhibitory Interactions in Localized Populations of Model Neurons. *Biophys. Journal*, **12**, 1972, 1–24.

[33] Wiskott, L. and von der Malsburg, C.: Face Recognition by Dynamic Link Matching. *In Sirosh, J., Miikkulainen, R., and Choe, Y., editors, Lateral Interactions in the Cortex: Structure and Function.* **Electronic book**, http://www.cs.utexas.edu/users/nn/web-pubs/htmlbook96.

List of Figures

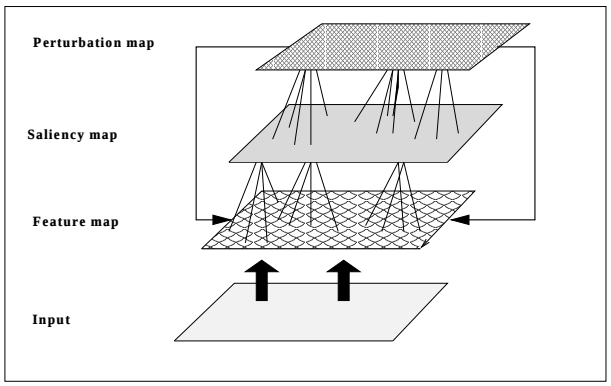

Figure 1: The system architecture

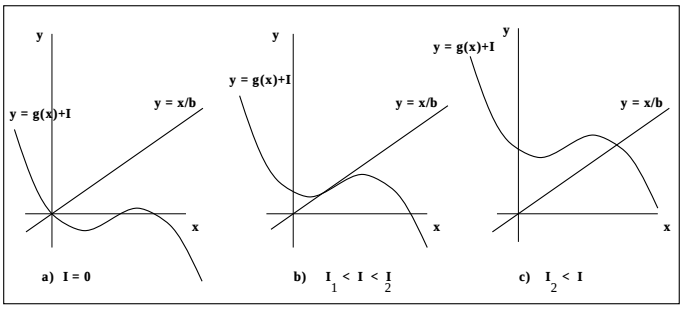

Figure 2: Phase plane nullclines of the FN system for different values of I. (a) For $I = 0$, the fixed point is globally stable; (b) the fixed point is unstable and a limit cycle solution is possible; (c) the fixed point is stable again.

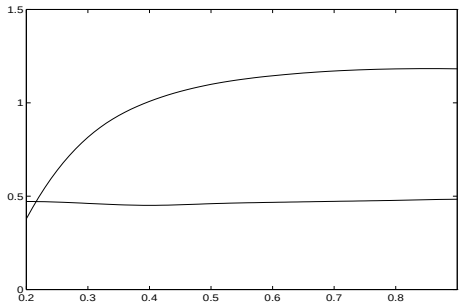

Figure 3: Amplitude and frequency of FN oscillator in function of I in a neighborhood of the bifurcation. The frequency is nearly constant while the amplitude is monotonic in I.

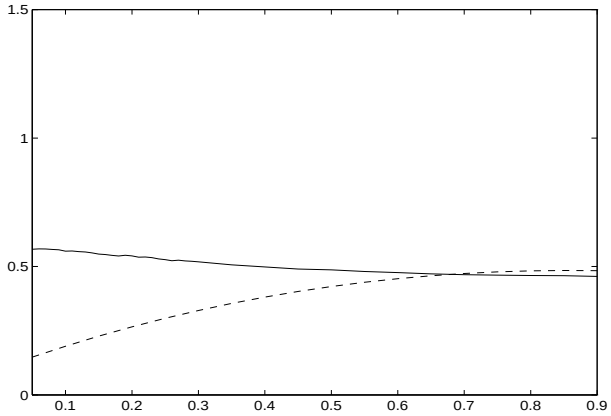

Figure 4: Amplitude (dashed curve) and frequency (solid curve) of a Wilson–Cowan oscillator as a function of I.

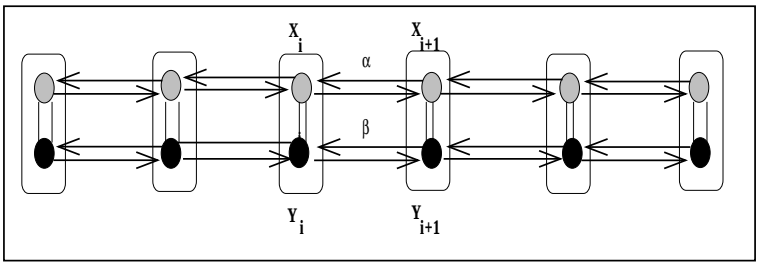

Figure 5: Connection topology between x and y units in a chain of FN oscillators.

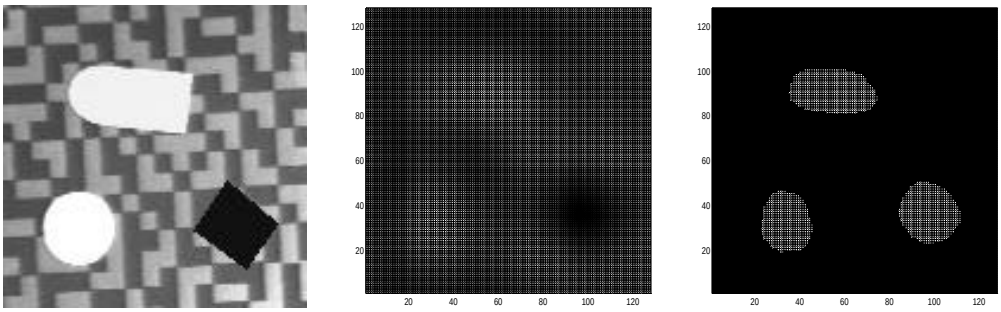

Figure 6: (left) An input image containing three salient objects over a textured background. (center) Amplitude map of the oscillators after a transient $T_a = 2 \cdot T$. (right) Output of saliency map; units belonging to salient regions have output $s_{ij} = 1$ while background units have zero output.

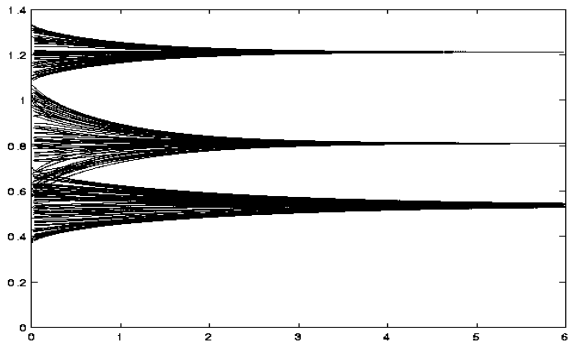

Figure 7: Temporal evolution of θ_{ij} components of perturbation map units $\mathbf{p}_{ij}$ according to system (18), for the input image shown in figure 6 (left).

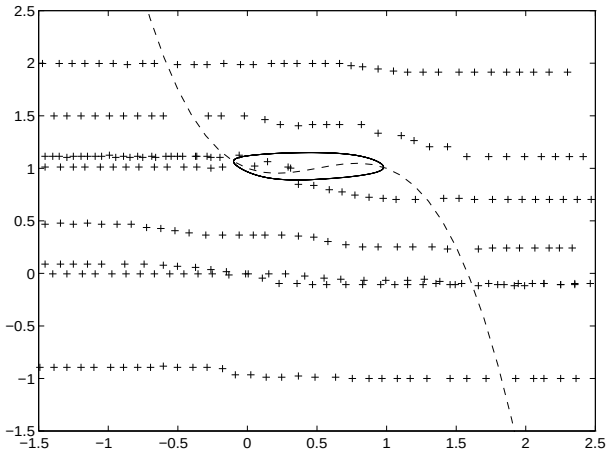

Figure 8: Isochrones of a FitzHugh-Nagumo oscillator ($I = 1, a = 0.1, b = 0.4$). Due to the relaxation property of the oscillator, the isochrones (curves denoted by crosses) are nearly horizontal except in the proximity of the cycle (solid curve) because the speed of variation of x relatively to y is very high far away from the cubic nullcline (dashed curve).

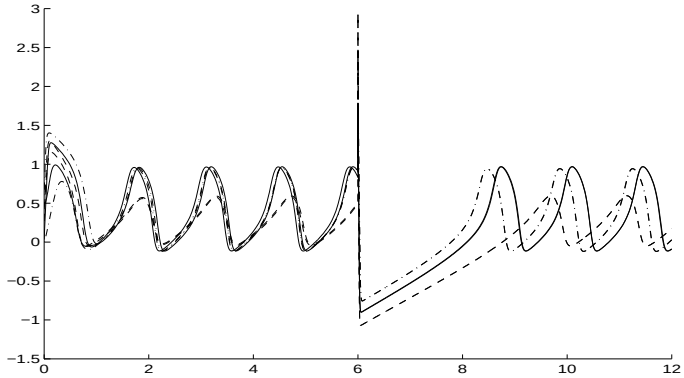

Figure 9: Temporal evolution of three pairs of oscillators belonging to the three salient objects in figure 6 (left) before and after perturbation at time $T_p = 4 \cdot T$. The additive perturbation desynchronizes the different groups of oscillators while those of a same group remain synchronous because shifted by the same amount.

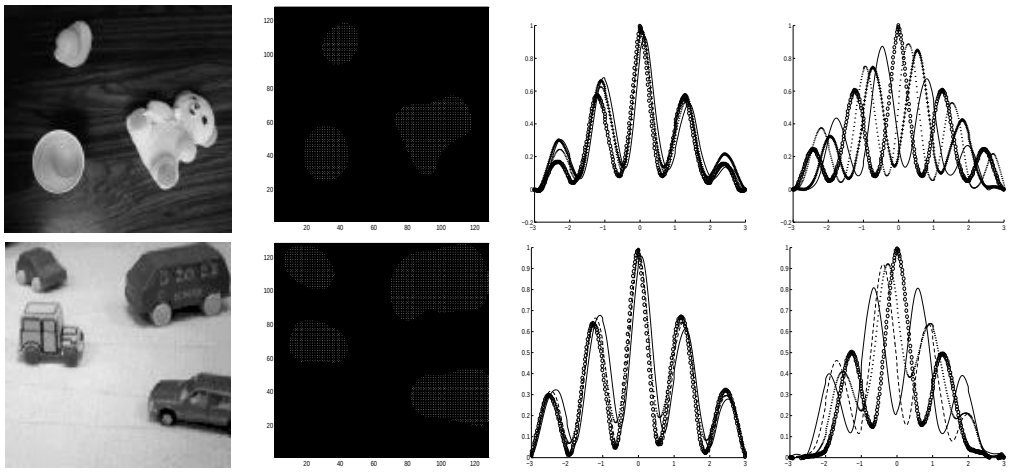

(a) (b) (c) (d)

Figure 10: Experimental results for two 128×128 grey-level images. (a) Input images; (b) attention maps; (c) cross-correlationdiagrams between pairs of units in different foreground objects for $t \in [2, 6]$ (before perturbation); (d) cross-correlation diagrams for $t \in [8, 12]$ (after perturbation). For comparison, the cross-correlation plots between two units in the same object are redrawn (open circles).

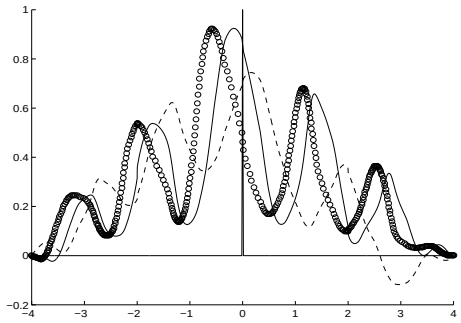

Figure 11: Cross-correlation diagrams between the three pairs of oscillators and the background.